

Supplementary Materials for

Poly(ADP-Ribose) (PAR) Binding to Apoptosis-Inducing Factor Is Critical for PAR Polymerase-1–Dependent Cell Death (Parthanatos)

Yingfei Wang, No Soo Kim, Jean-Francois Haince, Ho Chul Kang, Karen K. David, Shaida A. Andrabi, Guy G. Poirier, Valina L. Dawson,* Ted M. Dawson*

*To whom correspondence should be addressed. E-mail: tdawson@jhmi.edu (T.M.D.); vdawson@jhmi.edu (V.L.D.)

Published 5 April 2011, *Sci. Signal.* **4**, ra20 (2011)
DOI: 10.1126/scisignal.2000902

The PDF file includes:

Table S1. Primers used in sequential point mutation to construct single, double, triple, and quadruple point mutations.

Fig. S1. PAR binds to AIF.

Fig. S2. Alignment of the three putative PAR binding motifs in AIF.

Fig. S3. Determination of amino acids in AIF responsible for PAR binding.

Fig. S4. AIF and PAR binding affinity.

Fig. S5. Subcellular localization of AIF and PAR in cortical neurons.

Fig. S6. DNA and RNA are not involved in the PAR-AIF interaction.

Fig. S7. Pbm-AIF fails to bind to PAR and is resistant to its release from mitochondria in HeLa cells.

Fig. S8. Kinetics of AIF-mitochondria binding.

Fig. S9. Pbm-AIF is resistant to PARP-1–dependent cell death.

Table S1. Primers used in sequential point mutation to construct single, double, triple, and quadruple point mutations.

Mutant	Primer ID	Sequence
Single (Sm)	S-R588A AS-R588A	5' -CCGAATGCCAATTGCAGCGAAGATCATTAAAGGACGGTG-3' 5' -CACCGTCCTTAATGATCTTCGCTGCAATTGGCATTCCGG-3'
Di (Dm)	S-K589A AS-K589A	5' -GAATGCCAATTGCAGCGGCGATCATTAAAGGACGGTG-3' 5' -CACCGTCCTTAATGATCGCCGCTGCAATTGGCATTTC-3'
Triple (Tm)	S-K592A AS-K592A	5' -GCAGCGGCGATCATTGCGGACGGTGAGCAAC-3' 5' -GTTGCTCACCGTCCGCAATGATCGCCGCTGC-3'
Quadruple (Qm)	S-R583A AS-R583A	5' -GCTATGGAACGTCTTTAACGCAATGCCAATTGCAGCGG-3' 5' -CCGCTGCAATTGGCATTGCGTTAAAGACGTTCCATAGC-3'
AIFK254A	S-K254A AS-K254A	5' -CTCAGATTACCTTTGAAGCGTGCCTTGATTGCAACG-3' 5' -CGTTGCAATCAAGCACGCTTCAAAGGTAATCTGAG-3'
AIFR264A	S-R264A As-R264A	5' -CGGGAGGCACTCCAGCAAGTCTGTCTGCCATC-3' 5' -GATGGCAGACAGACTTGCTGGAGTGCCTCCCG-3'
AIFR588L;K 589L	S-RK589L AS-RK589L	5' -CCGAATGCCAATTGCACTGCTGATCATTAAAGGACGGTG-3' 5' -CACCGTCCTTAATGATCAGCAGTGCAATTGGCATTCCGG-3'
AIFR588L;K 592L	S-RK592L AS-RK592L	5' -CCGAATGCCAATTGCACTGAAGATCATTCTGGACGGTGAGCAACATGAAG-3' 5' -CTTCATGTTGCTCACCGTCCAGAATGATCTTCAGTGCAATTGGCATTCCGG-3'
AIFK589L;K 592L	S-KK592L AS-KK592L	5' -CCGAATGCCAATTGCAAGGCTGATCATTCTGGACGGTGAGCAACATGAAG-3' 5' -CTTCATGTTGCTCACCGTCCAGAATGATCAGCCTTGCAATTGGCATTCCGG-3'
AIFR588L;K 589L;K592L	S-RKK592L AS-RKK592L	5' -CCGAATGCCAATTGCACTGCTGATCATTCTGGACGGTGAGCAACATGAAG-3' 5' -CTTCATGTTGCTCACCGTCCAGAATGATCAGCAGTGCAATTGGCATTCCGG-3'

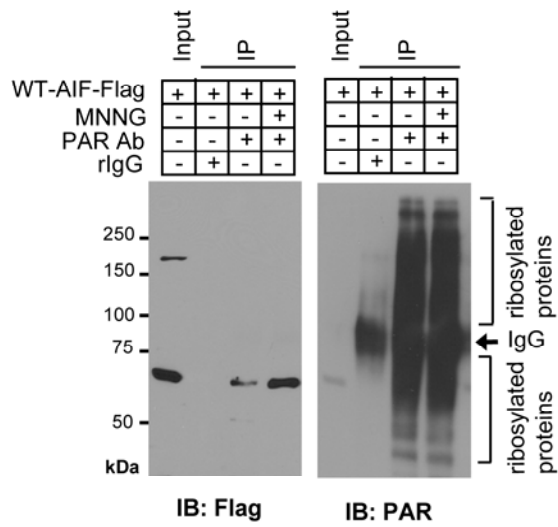
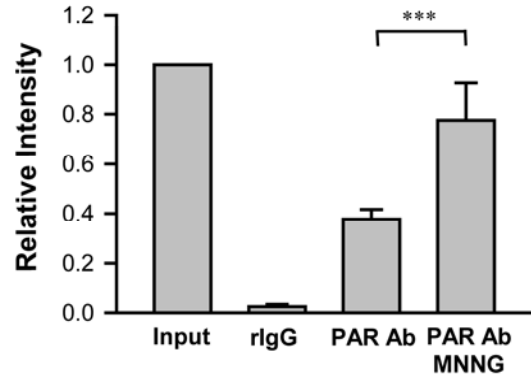
A**B**

Fig. S1. PAR binds to AIF. (A) Co-immunoprecipitation of WT-AIF-Flag with PAR in post-nuclear fractions isolated from HeLa cells 2 h after MNNG treatment (50 μ M for 15 min). rIgG, rabbit IgG. (B) The intensity of AIF signal was quantified and normalized to input (right panel). *** $p < 0.001$, by one-way ANOVA analysis, $n = 3$.

Mouse	(Q9Z0X1)	222	GGVAVLTG	KKVV HLDVRGNMVKL	244
Human	(O95831)	223	GGVAVLTG	KKVV QLDVRDNMVKL	245
Rat	(Q9JM53)	222	GGVAVLTG	KKVV HLDVRGNMVKL	244
Chicken	(NP001007491)	201	GGVAVLSG	KKVV HMDVRGNTVKL	223
PAR-binding Consensus			[.K/R..].XHX BXHHBBHHBX ..		
Mouse	(Q9Z0X1)	441	FYDI	KLGR RRVEHHDHAVVSGRL	463
Human	(O95831)	442	FYDI	KLGR RRVEHHDHAVVSGRL	464
Rat	(Q9JM53)	441	FYDI	KLGR RRVEHHDHAVVSGRL	463
Chicken	(NP001007491)	420	FYDI	KLGR RRVEHHDHAVVSGRL	442
<i>Drosophila</i>	(Q9VQ79)	568	FFDPLLGR	RR VEHHDHSSVVSRL	590
PAR-binding Consensus			[.K/R..].XHX BXHHBBHHBX ..		
Mouse	(Q9Z0X1)	567	LRDKVVVGIVLWNVFN	RMPIARKIIK	592
Human	(O95831)	568	LRDKVVVGIVLWNI FN	RMPIARKIIK	593
Rat	(Q9JM53)	567	LRDKVVVGIVLWNVFN	RMPIARKIIK	592
Chicken	(NP001007491)	546	LRDKVVVGIVLWNI FN	RMPIARKIIK	571
<i>Drosophila</i>	(Q9VQ79)	695	LKNDKIVGILLWNLFN	RIGLARTII	719
PAR-binding Consensus			[.K/R..].XHX BXHHBBHHBX ..		

Fig. S2. Alignment of the three putative PAR binding motifs in AIF. The three putative PAR-binding motifs of mouse, human, rat, and chicken are indicated and aligned. The amino acid number is indicated on the right and left of the amino acid sequence. Accession numbers are in parentheses. The PAR-binding consensus sequence ([.K/R..].XHX**BXHHBBHHBX**..), which comprises approximately 20 amino acids and is characterized by the presence of hydrophobic amino acids (H;ACGVILMFYW) spaced by basic amino acids (B; HKR) and by an accumulation of basic amino acid residues at the N-terminal site of the motif (KR), is indicated below each putative site. Conserved basic residues within the three putative PAR-binding sites are indicated in red.

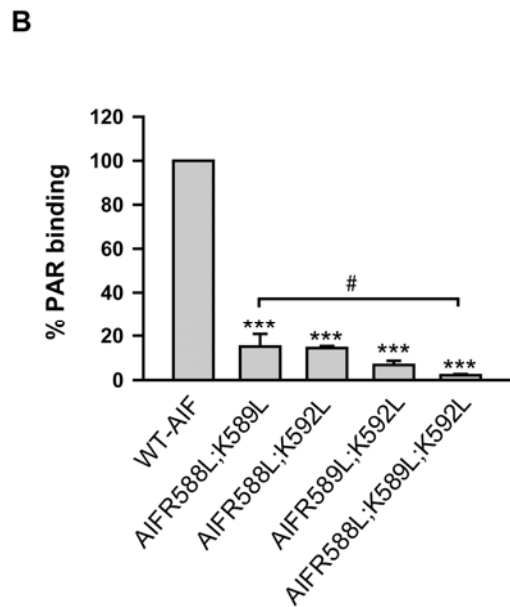
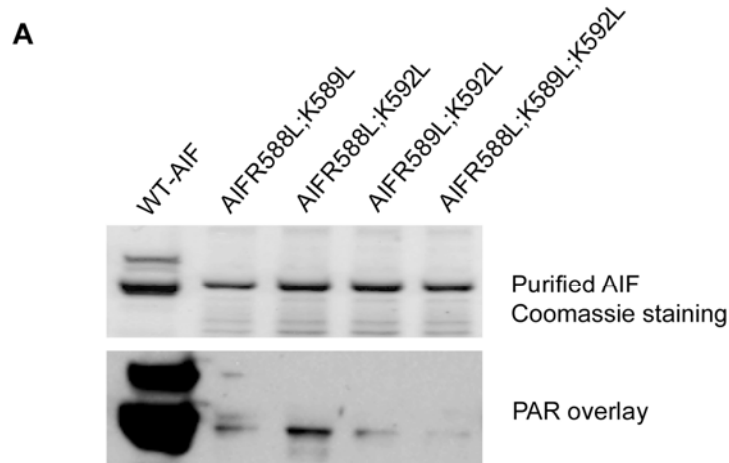


Fig. S3. Determination of amino acids in AIF responsible for PAR binding. (A) Three basic amino acids (R588, K589, K592) residing in the PAR binding consensus sequence were sequentially mutated to leucine. His-tagged WT-AIF and mutant AIF proteins were purified from *E.coli* (upper panel) and analyzed for PAR binding activity by the PAR overlay assay using purified PAR. (B) The radioactive signal was quantified and normalized to WT-AIF (lower panel), *** $p < 0.001$; # $p < 0.05$, by one-way ANOVA analysis. $n = 4$.

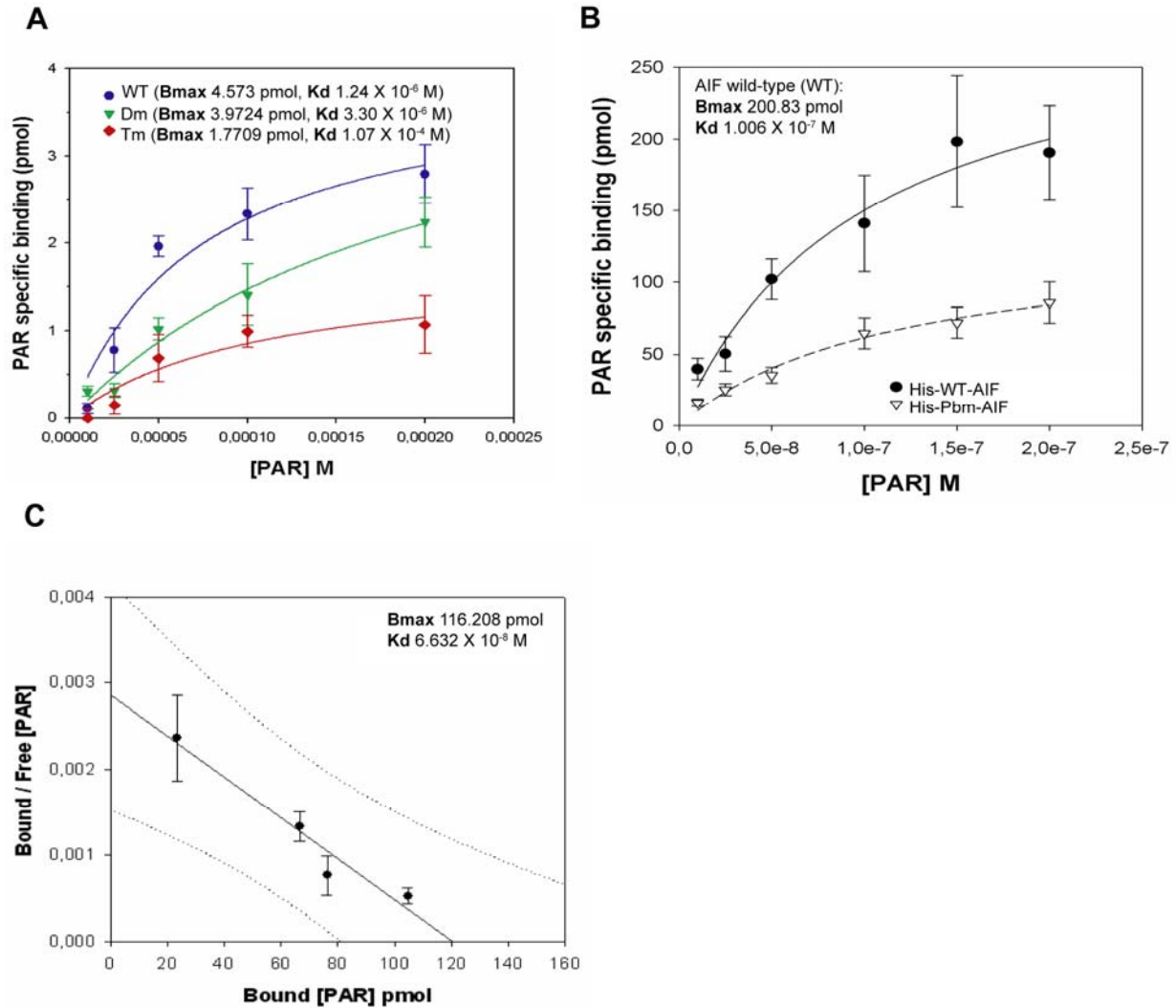


Fig. S4. AIF and PAR binding affinity. (A) The binding affinity constant (Kd) and maximum binding capacity (Bmax) of AIF mimetic peptides, WT (amino acids 567-592), Dm (amino acids 567-587-R588A-K589A-590-592), Tm (amino acids 567-587-R588A-K589A-590-K592A) were determined by the nitrocellulose binding assay. Kd and Bmax are indicated, $n = 3$. (B) Analysis of PAR binding properties of full-length His tagged wild type (WT)-AIF-Flag and His-tagged PAR binding mutant (Pbm)-AIF-Flag. Kd and Bmax are indicated. The PAR-binding affinity of the Pbm-AIF is almost linear and likely reflects non-specific binding, $n = 6$. (C) Scatchard plot of the specific binding of mouse AIF to PAR polymer with a 95% confidence interval (*dotted line*). Kd and Bmax are indicated, $n = 6$.

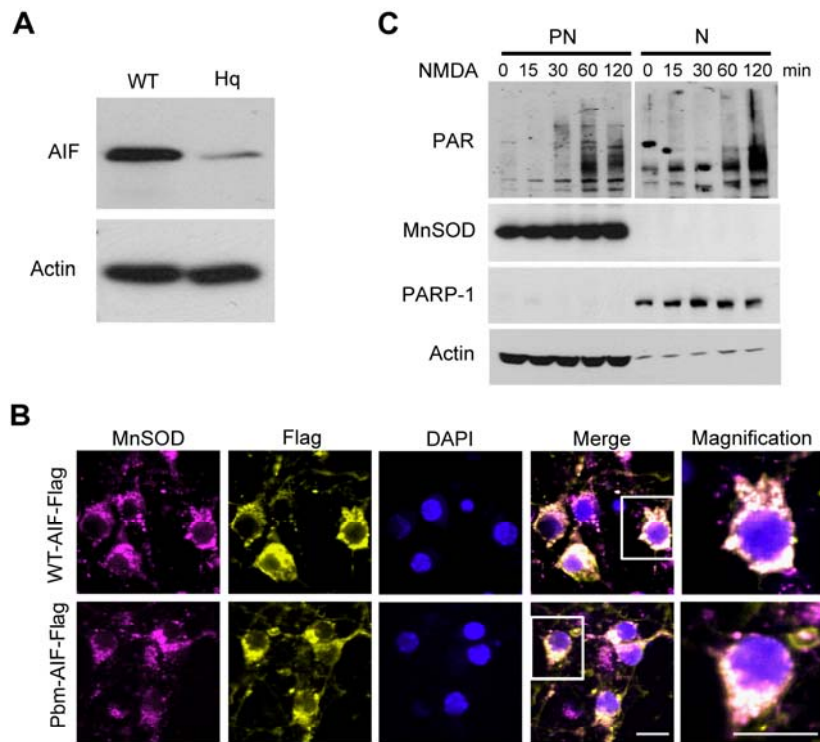


Fig. S5. Subcellular localization of AIF and PAR in cortical neurons. (A) Endogenous AIF detected by immunoblot with an anti-AIF antibody in WT and Hq primary cortical neuronal cultures. Anti-actin was included as an indicator for equal loading, $n = 3$. (B) Mitochondrial location of exogenous WT-AIF-Flag and Pbm-AIF-Flag in Hq primary cortical neuronal cultures. Cells were immunostained with the mitochondrial protein MnSOD (pink) and AIF-Flag (yellow). Nuclei were counterstained with DAPI (blue). White indicates overlap between MnSOD and AIF staining. Scale bar, 10 μm . Images are representative for at least 4 independent experiments. (D) Both endogenous WT-AIF and exogenous Pbm-AIF translocated to the nucleus 24 h after 100 nM staurosporine treatment. The nuclear fraction was prepared from cortical neurons infected with Pbm-AIF. The purity of nuclear fraction was confirmed by both nuclear and mitochondria makers, Histone H3 and Tom20, respectively. (C) PARP-1 activity in cortical neurons. After NMDA (500 μM , 5 min) administration, postnuclear (PN) and nuclear (N) fractions were isolated as indicated (0-120 min) after NMDA treatment. PARP-1 activity was determined by PAR immunoblotting. The integrity of cellular fractions was determined by the mitochondrial marker MnSOD and the nuclear marker PARP-1. Actin serves as internal loading control, $n = 3$.

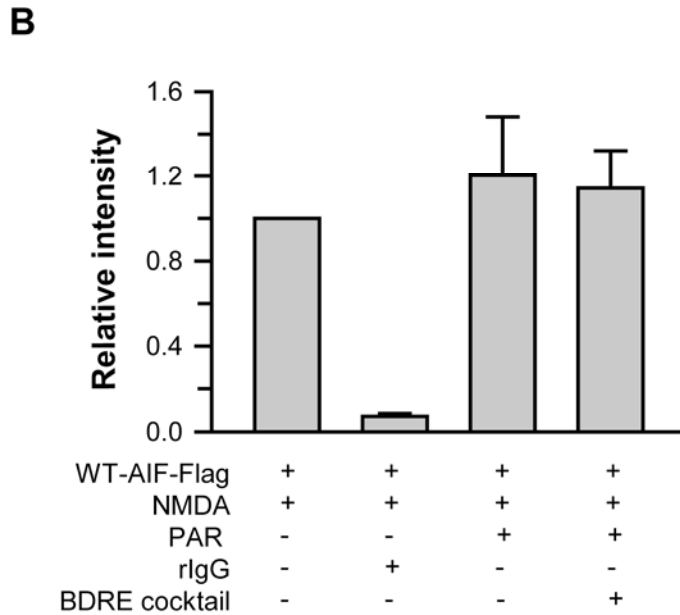
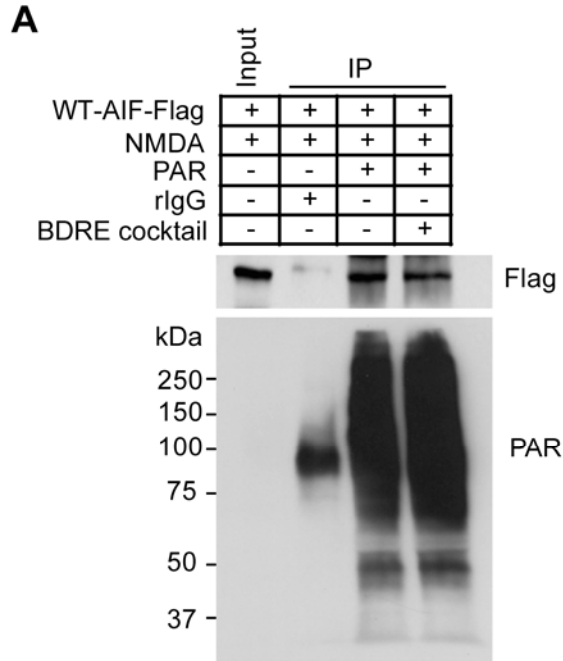


Fig. S6. DNA and RNA are not involved in PAR-AIF interaction. (A) Co-immunoprecipitation of PAR with WT-AIF-Flag in cortical neurons. Postnuclear proteins were isolated 2 h after NMDA treatment (500 μ M for 5 min) and precipitated by the anti-PAR antibody in the absence or presence of BDRE cocktail containing 1 mg/ml benzonase, 4 U/ml DNase I, 10 mg/ml RNase A, and 0.5 μ g/ml ethidium bromide. The immunoblot was probed with an anti-Flag antibody and reprobed with the anti-PAR antibody. Rabbit IgG (rIgG) serves as a negative control. (B) The intensity of the Flag signal was quantified and normalized to input, $n = 3$.

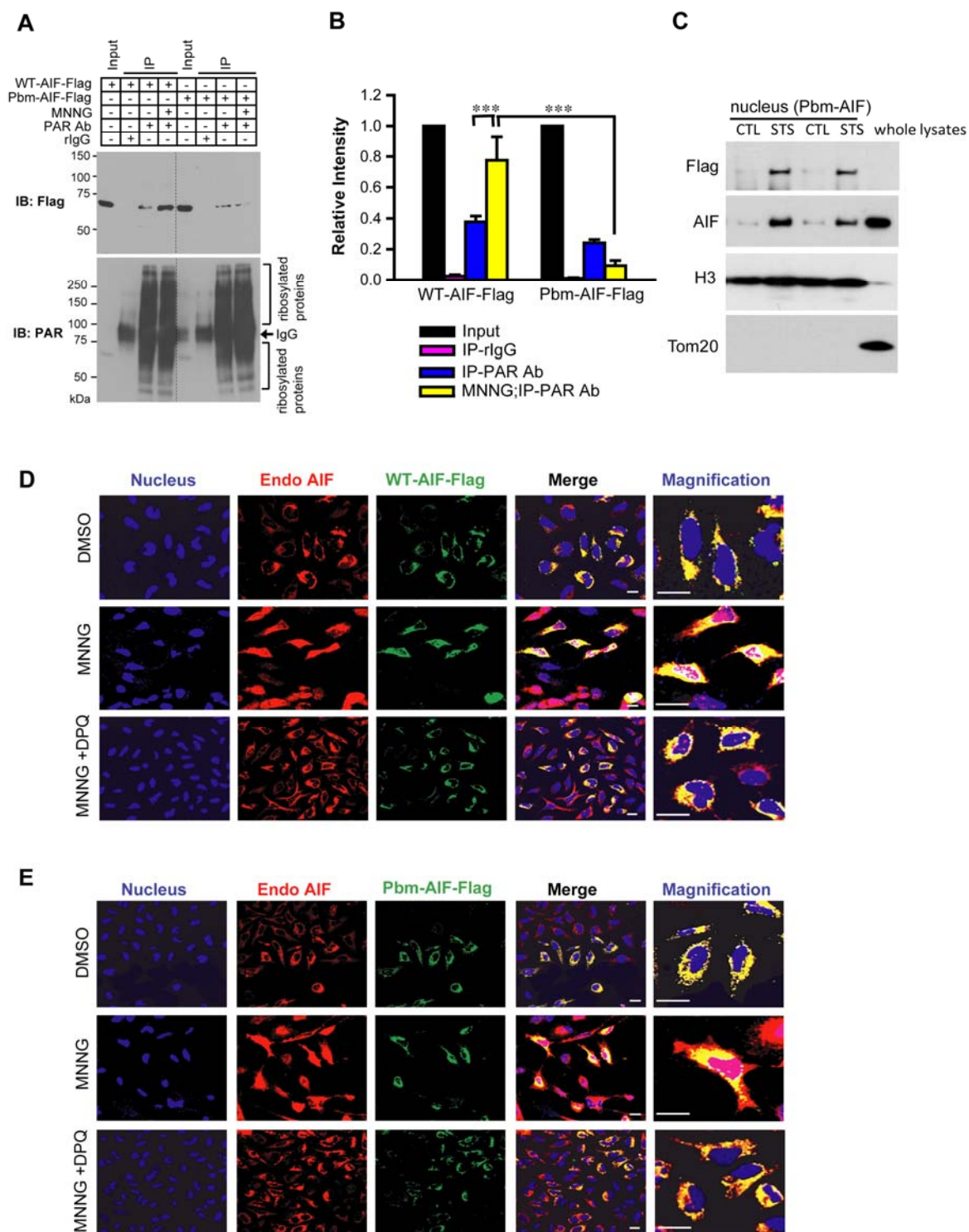


Fig. S7. Pbm-AIF fails to bind to PAR and is resistant to its release from mitochondria in HeLa cells. (A) Co-immunoprecipitation of endogenous PAR with WT-AIF, but not Pbm-AIF

in HeLa cells stably expressing either WT-AIF-Flag or Pbm-AIF-Flag. Postnuclear proteins were isolated 2 h after MNNG treatment (50 μ M for 15 min) and precipitated by the anti-PAR antibody. The immunoblot was probed with an anti-Flag antibody and reprobed with the anti-PAR antibody. Rabbit IgG (rIgG) serves as a negative control. **(B)** The intensity of Flag signal was quantified and shown as a histogram. Input of WT-AIF-Flag, Pbm-AIF-Flag was regarded as 1, respectively. *** $p < 0.001$, $n = 3$. **(C)** Both endogenous WT-AIF and exogenous Pbm-AIF translocated to the nucleus 24 h after 100 nM staurosporine (STS) treatment. The nuclear fraction was prepared from cortical neurons infected with Pbm-AIF. The purity of nuclear fraction was confirmed by both nuclear and mitochondria makers, Histone H3 and Tom20, respectively. CTL, control. **(D)** AIF nuclear translocation was determined 4 h after MNNG treatment (50 μ M for 15 min) in the presence or absence of DPQ (30 μ M) in HeLa cells by immunofluorescence. Endogenous AIF is shown in red. Exogenous AIF (WT-AIF-Flag) was detected by an anti-Flag antibody (Green). Note that both endogenous and exogenous AIF translocate to the nucleus following MNNG treatment and the PARP inhibitor, DPQ prevents the translocation. In the merged images, yellow indicates overlap between endogenous and exogenous AIF. Pink indicates the overlap of endogenous AIF and nucleus. Scale bar, 20 μ m. **(E)** AIF nuclear translocation was determined 4 h after MNNG treatment (50 μ M for 15 min) in the presence or absence of DPQ (30 μ M) in HeLa cells by immunofluorescence. Endogenous AIF is shown in red. Exogenous AIF (Pbm-AIF-Flag) was detected by Flag antibody (Green). Note that only endogenous and but not exogenous AIF translocates to the nucleus following MNNG treatment and the PARP inhibitor, DPQ prevents the translocation. In the merged images, yellow indicates overlap between endogenous and exogenous AIF. Pink indicates the overlap of endogenous AIF and nucleus. Scale bar, 20 μ m.

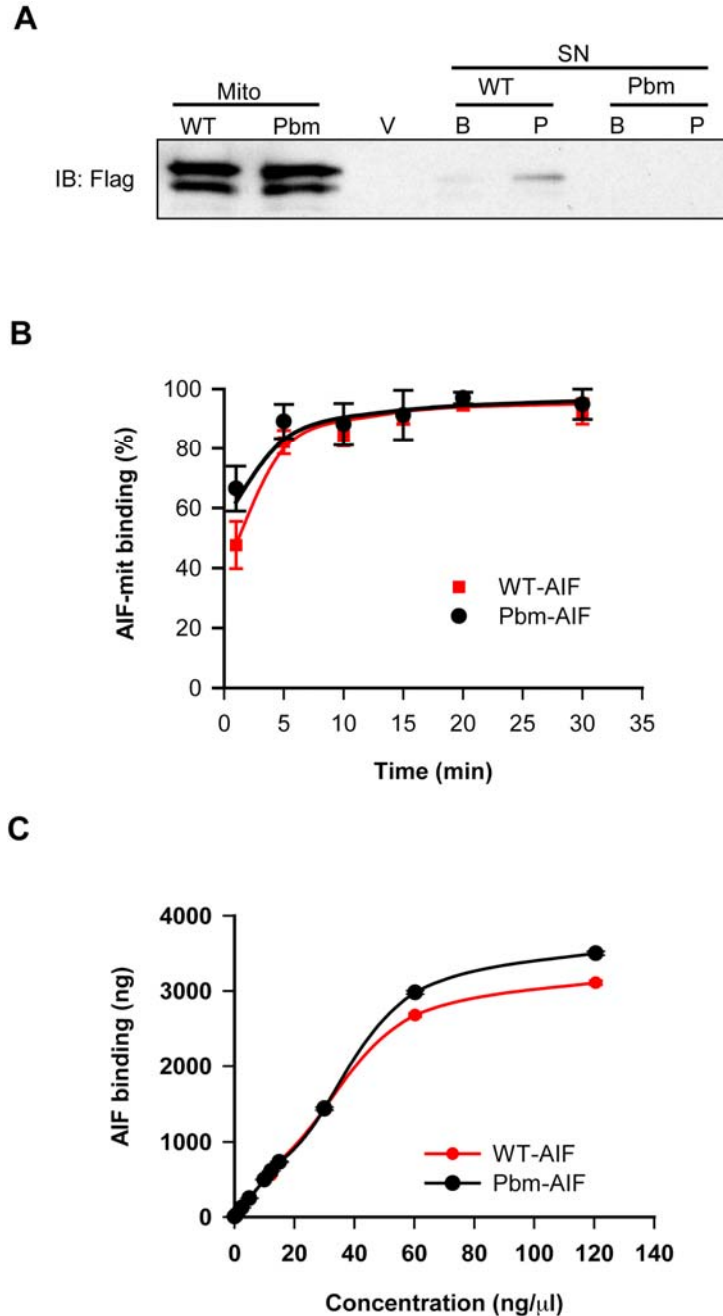


Fig. S8. Kinetics of AIF-mitochondria binding. (A) Mitochondria isolated from HeLa cells expressing WT-AIF-Flag (WT) or Pbm AIF-Flag (Pbm) protein were incubated with PAR (80 nM) at room temperature for 30 min. The levels of AIF were determined in the supernatant. B indicates buffer only; P indicates PAR, $n = 3$. (B) Recombinant WT-AIF (2.5 ng/ml) and Pbm-AIF (2.5 ng/μl) were incubated with isolated mitochondria (200 μg/ml) for 1 min, 5 min, 10 min, 15 min, 20 min or 30 min. The levels of AIF were determined in the supernatant. (C) Isolated mitochondria (200 μg/ml) were incubated with different concentrations of recombinant WT-AIF and Pbm-AIF varying from 0.1 ng/μl to 120.5 ng/μl at room temperature for 30 min. The levels of AIF were determined in the supernatant.

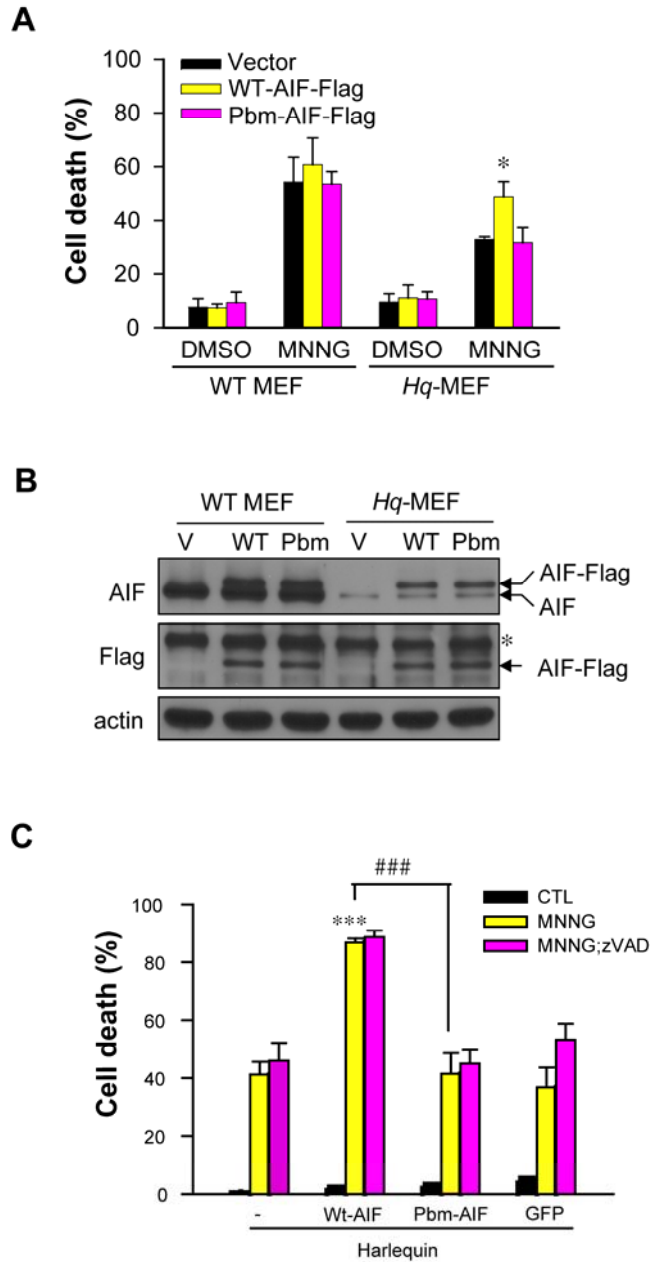


Fig. S9. Pbm-AIF is resistant to PARP-1-dependent cell death. (A) The effect of WT-AIF-Flag or Pbm-AIF-Flag on WT and Hq MEF cell viability was determined 24 h after MNNG cytotoxicity (500 μ M for 15 min), $*p < 0.05$, $n = 3$. (B) WT-AIF-Flag and Pbm-AIF-Flag were equally expressed in MEF cells. * indicates a nonspecific band. (C) The effect of WT-AIF-Flag or Pbm-AIF-Flag on Hq MEF cell viability was determined 24 h after MNNG (500 μ M for 15 min) cytotoxicity with and without zVAD (100 μ M), $***p < 0.001$, $###p < 0.001$, by one-way ANOVA analysis, $n = 3$. CTL, control.